arXiv:1703.04551v1 [physics.ins-det] 9 Mar 2017

A procedure for detecting hidden surface defects in a plate from real thermal data by means of active thermography

Gabriele Inglese*[1], Roberto Olmi †[2], and Saverio Priori[2]

[1]IAC 'M. Picone" - CNR, Via Madonna del Piano 10, 50019 Sesto Fiorentino (Italy)
[2]IFAC - CNR, Via Madonna del Piano 10, 50019 Sesto Fiorentino (Italy)

Abstract Let Ω_ϵ be a metallic plate whose top inaccessible surface has been damaged by some chemical or mechanical agent. We heat the opposite side and collect a sequence of temperature maps u^ϵ. Here, we construct a formal explicit approximation of the damage $\epsilon\theta$ by solving a nonlinear inverse problem for the heat equation in three steps: (i) smoothing of temperature maps, (ii) domain derivative of the temperature, (iii) thin plate approximation of the model and perturbation theory.

Our inversion formula is tested with realistic synthetic data and used in a real laboratory experiment.

1 Introduction.

Active thermography is a non-contact, non-destructive technique exploiting the information contained in the thermal contrast to gain knowledge about the integrity of a material structure.

Since any material object is subject to aging, monitoring the deterioration is an essential task. In particular, corrosion of metallic structures poses a huge problem to the maintenance of industrial and public assets like steel bridges, chemical and nuclear power plants, pipelines and others.

Nondestructive testing plays a crucial role in the effort of an early detection of the decay of metal structures. Applications of thermography have been reported, for example, in the diagnostics of aircraft structures [1] [2], in the integrity analysis of pipelines [3], in the detection of cracks in steel bridges [4]

*gabriele@fi.iac.cnr.it
†r.olmi@ifac.cnr.it

and, in general, in the investigation of thick metallic structures [5] [6].

In this paper we process thermal data to evaluate inaccessible surface damages on a plate made of a heat-conducting material. In particular, we obtain an explicit approximation of the damage by means of perturbative methods.

For simplicity, we deal with a flat geometry. The undamaged plate is modeled by the parallelepiped $\Omega_0 = \{(x, y, z) \in (-\frac{L}{2}, \frac{L}{2}) \times (-\frac{L}{2}, \frac{L}{2}) \times (0, a)\}$ $(0 < a \ll L)$. Let $c\rho$ be the volumetric heat capacity (c is the specific heat capacity and ρ is the density) and κ be the thermal conductivity. The specimen is assumed homogeneous and isotropic so that c, ρ and κ are positive scalar constants. We refer to [13] for a complete background about the classical theory of heat.

Suppose that Ω_0 divides an *outer* aggressive environment from our laboratory. Let $S_{Top} = \{(x, y, a) \;\; x, y \in [-\frac{L}{2}, \frac{L}{2}]\}$ be the inaccessible face of Ω_0 in contact with the environment while $S_{Bot} = \{(x, y, 0) \;\; x, y \in [-\frac{L}{2}, \frac{L}{2}]\}$ is the laboratory side. We are able to heat the specimen Ω_0 with a device (a couple of $1000W$ spotlights in our case) that produces a heat flux $\phi(x, y)$ through S_{Bot} for a time interval $(0, T_{max})$. In the meanwhile, the increase of surface temperature on S_{Bot} is monitored by means of an infrared camera. A sequence of temperature maps is stored.

Let $u^0(x, y, z, t)$ be the temperature at the point $(x, y, z) \in \Omega_0$ at time t (*background temperature* at time t).

In this framework, we suppose that a damage, due to chemical or mechanical aggression could appear on the top side. The damaged specimen is called Ω_ϵ. The temperature maps of the bottom side of Ω_ϵ are $u_k^\epsilon = u^\epsilon(x, y, 0, t_k)$ for $0 < t_1 < t_2 < ... < t_N \leq T_{max}$. Our goal is to identify the damage from the knowledge of the *thermal contrast*

$$u^\epsilon(x, y, 0, t_k) - u^0(x, y, 0, t_k)$$

for $0 < t_1 < t_2 < ... < t_N \leq T_{max}$.

This procedure is called Stepped Heating Thermography (SHT: see for example [23] Section 9.3). A technical and historical introduction to Thermal NonDestructive Testing is in the Preface of [23]. In Table 1.2 of [23] a detailed list of applications is reported. In particular, SHT is mainly used in the thermal testing at low conductivities or to check composite materials (carbon fiber-reinforced plastic, chips, adhesive). Here, we apply SHT to the NDT of plates with both high and low conductivity.

Nomenclature:

Parameters

Ω_0 undamaged plate

Ω_ϵ damaged plate
S_{Top} surface of Ω_0 in contact with environment (inaccessible)
S_{Bot} laboratory side of Ω_0
ϵ depth of the damage
θ shape of the damage
U^0 initial and environmental temperature
h heat transfer coefficient
ϕ heat flux density
T_{max} time length of the experiment
κ conductivity
ρ density
c specificific heat capacity
$\alpha = \frac{\kappa}{\rho c}$ diffusivity

Acronymos

IBVP Initial Boundary Value Problem
IP Inverse Problem
TPA Thin Plate Approximation
FEM Finite Elements Method

1.1 The Inverse Problem

We have assumed that the only effect of the external aggression to the specimen is the loss of an amount of matter so that S_{Top} becomes an unflat surface (see for example [8], [10], [22]). Furthermore, we suppose that a nonnegative function $\epsilon\theta$ describes the deviation of damaged S_{Top} from original plane. More precisely,

$$\Omega_\epsilon = \{(x, y, z) : x, y \in (-\frac{L}{2}, \frac{L}{2}); z < a - \epsilon\theta(x, y)\}.$$

We can formulate the inverse problem **IP**:

IP Detect and evaluate $\epsilon\theta$ from the knowledge of ϕ (controlled heat flux) and $u^\epsilon(x, y, 0, t_k) - u^0(x, y, 0, t_k)$ for $k = 1, ..., N$ (maps of the thermal contrast).

We point out that the heat flux ϕ through S_{Bot} is actually unknown because of factors like surface reflection of electromagnetic radiation and dispersion of heat in the air between lamps and plate. For this reason, in practice we must identify ϕ from the temperature maps taken with the infrared camera which, ultimately, are the only available data (see section 3).

Remarks about how we model damages

1. The defect is described by a function. A surface defect is naturally modeled by means of a function of two variables when it is originated by mechanical

collisions or some kind of corrosion (for example, uniform corrosion or erosion-corrosion). On the other hand, pitting corrosion or cracking (see for example [21] (section 1.5)) must be modeled by means of a curve that is not the graph of a function ([12]).

2. The defect is actually time-independent. Although the formation of defects on S_{Top} is a dynamical process, we model it by means of a time-independent function $\epsilon\theta$. It is correct as long as the time scale of damaging evolution is much larger than the observation time T_{max}.

1.2 Details of the direct model

The temperature in Ω_ϵ for $t \in (0, T_{max}]$, fulfills the heat equation

$$u_t = \alpha \Delta u \tag{1}$$

with boundary conditions that account for energy exchanges between the specimen and the environment:

$$\kappa u_n(\sigma, t) + h(u(\sigma, t) - U^0) - \phi(\sigma) = 0 \tag{2}$$

where $\sigma \in \partial\Omega_\epsilon$. These are called Robin or third kind boundary conditions. Initial data is

$$u(x, y, z, 0) = U_{in}(x, y, z, 0). \tag{3}$$

Here, u_n is the outward normal derivative (normal with respect to the boundary $\partial\Omega_\epsilon$) and $\alpha = \frac{\kappa}{c\rho}$ is the diffusivity. The heat exchange coefficient h is related to the geometry of the specimen and to the environmental condition close to S_{top}. We assume: $h > 0$ is constant at S_{top}; $h = 0$ on the vertical sides and on the bottom side of the plate. The incoming heat flux ϕ is concentrated at S_{Bot}. Finally, we suppose that U^0 is the same on S_{Bot} and on S_{Top} and that the initial temperature is $U_{in}(x, y, z) = U^0$.

1.3 Identification of the background temperature

We have already observed, talking of the flux in subsection 1.1, that the only data available in practice are the maps of the bottom side of damaged specimen, recorded by the infrared camera. In fact we expect that, at least for $t < t_0$, the temperature of S_{bot} is independent of $\epsilon\theta$ with the exception of a small portion of the side just below the damaged area. Hence the background temperature in Ω_0 is recovered from the knowledge of $u^\epsilon(x, y, 0, t_k)$.

If the flux density $\phi = \phi_0$ is constant in space and time (this is the case of *stepped heating* or *long pulse* thermography), the temperature $u^0 = u^0(z, t)$ is independent of x and y. Indeed, it can be computed as a series dependent on z and t [13]:

$$u^0(z,t) = \frac{\phi}{h}\left[1 + \lambda\left(1 - \frac{z}{a}\right) - \sum_{n=1}^{\infty} \frac{2\lambda\left(\beta_n^2 + \lambda^2\right) cos\left(\beta_n z/a\right)}{\beta_n^2\left(\lambda + \lambda^2 + \beta_n^2\right)} e^{-\beta_n^2 \tau}\right] \quad (4)$$

where $\lambda = ah/\kappa$, β_n are the real roots of $\beta tan\beta = \lambda$ and $\tau = \alpha t/a^2$.

As the n_{th} root β_n belongs to the interval $[(n-1)\pi, (2n-1)\pi/2]$, small times (a few seconds) bring to very large exponents in (4) for $n > 1$, for the assumed values of the physical and geometrical parameters α, κ, h and a. Therefore, the first term of the series (4) gives a sufficiently good approximation of the background temperature.

For low values of κ (negligible longitudinal heat transfer) and t (negligible dependence on h before a time $t_a > 0$), equation (4) can be used successfully for recovering ϕ from u^0. It gives us a complete quantitative information about the heat flux.

1.4 Main result in 2D: explicit approximation of the damage

The Initial Boundary Value Problem (IBVP) defined by (1) (2) (3) is well posed (see for example [24, Chapter 2]) and we refer to it as to the Direct Model underlying **IP**. On the other hand, in spite of recent uniqueness results by Isakov (see [20]), **IP** has a close relation with the Cauchy problem for the heat equation which is severely ill-posed because its solutions are highly unstable (see for example [7] Chapter 4).

First, we linearize the inverse problem by means of Domain Derivative, a technique that accounts for smallness of ϵ (the size of the damage) with respect to the thickness a of the plate. Let u^ϵ denote the unique solution of IBVP (1), (2), (3). We choose this notation to point out the nonlinear dependence of the solution on $\epsilon\theta$. The Domain Derivative u' is defined as the (Gateaux) derivative of u^ϵ with respect to the parameter ϵ in the direction θ at $\epsilon = 0$.

It comes from straightforward calculations (reported in detail in [9]) and linearity arguments that the function $w \equiv \epsilon u'$ $(\forall \epsilon > 0)$ fulfills the following IBVP in $\Omega_0 \times (0, T]$

$$c\rho w_t = \kappa \Delta w \quad (5)$$

with boundary conditions of the form

$$\kappa w_z(x,a,t) + hw(x,a,t) = \epsilon\theta(x)(\kappa u^0_{zz}(x,a,t) + hu^0_z(x,a,t)) - \epsilon\theta_x(x)\kappa u^0_x(x,a,t) \quad (6)$$

$$\kappa w_z(x,0,t) = 0 \quad (7)$$

and initial data

$$w(x,z,0)=0. \tag{8}$$

We rescaled u' by the parameter ϵ because $\epsilon\theta$ is actually the damage that we must recover and $w(x,0,t)=\epsilon u'(x,0,t)$ is the first order approximation of the thermal contrast $u^{\epsilon}(x,0,t)-u^{0}(x,0,t)$ that we actually measure.

Then, we use the thinness of the plate itself to expand the unknown and the data in powers of a (see the Appendix for details). In fact, after scaling the variables z, the scaled Domain Derivative w in $(-\frac{L}{2},\frac{L}{2})\times(0,1)\times(0,T_{max}]$ fulfills the parabolic equation

$$a^2\frac{w_t}{\alpha}=a^2w_{xx}+w_{zz} \tag{9}$$

with boundary conditions

$$\kappa w_z(x,1,t)+ahw(x,1,t)=a\epsilon\theta(x)(hu^0_z(x,a,t)+\kappa u^0_{zz}(x,a,t))-a\epsilon\theta_x(x)\kappa u^0_x(x,a,t) \tag{10}$$

$$\kappa w_z(x,0,t)=0 \tag{11}$$

$$w_x(-L/2,z,t)=w_x(L/2,z,t)=0 \tag{12}$$

(adiabatic conditions on the vertical sides) and initial data

$$w(x,z,0)=0. \tag{13}$$

Plugging the formal expansions

$$w=w_0+aw_1+a^2w_2+O(a^3) \tag{14}$$

$$\theta=\theta_0+a\theta_1+a^2\theta_2+O(a^3) \tag{15}$$

into the IBVP above and applying perturbation theory, (see Appendix for details) we obtain an explicit relationship between the unknown coefficients $\theta_j(x,t)$ and the thermal contrast approximated by means of the domain derivative $w(x,0,t)$. If the flux density ϕ is constant in space and time, we have

$$\begin{aligned}
\epsilon\theta_0(x,t)&=\frac{hw(x,0,t)}{D(t)}\\
\epsilon\theta_1(x,t)&=\frac{c\rho w_t(x,0,t)-\kappa w_{xx}(x,0,t)}{D(t)}\\
\epsilon\theta_2(x,t)&=\frac{h}{2\kappa}\frac{c\rho w_{0t}-\kappa w_{0xx}}{D(t)}\\
\epsilon\theta_3(x,t)&=\frac{1}{3}\frac{c\rho w_{2t}-\kappa w_{2xx}}{D(t)}\\
&=\frac{1}{6\alpha}(\epsilon\theta_{1t}(x,t)D(t)+\epsilon\theta_1(x,t)D_t(t))-\frac{1}{6}D\epsilon\theta_{1xx}(x,t).
\end{aligned} \tag{16}$$

where $D(t)=hu^0_z(a,t)+c\rho(a,t)u^0_t(a,t)$.

We test our method with synthetic data in section 2 and then we apply it to the reconstruction of a real damage on the hidden face of an aluminum plate (section 4). Numerical differentiation of discrete data is carried out successfully by means of smoothing techniques and local weighted regression [14].

2 Test on the inversion formula with synthetic data

Let Ω_0 be the rectangle $[-L/2, L/2] \times [0, a]$. We test the explicit formula (15,16) on a damaged boundary $a - \epsilon\theta$ where $\theta(x)$ is one of the following:

- an unimodal gaussian function: $e^{-\gamma x^2}$
- a rectangular function: $rect(x, d) = H(x + \frac{d}{2}) - H(x - \frac{d}{2})$, defined in terms of the *Heaviside* function $H(x)$
- a bimodal gaussian function: $A_1 e^{-\gamma_1 (x-x_1)^2} + A_2 e^{-\gamma_2 (x-x_2)^2}$

Our data consist of $u^\epsilon(x, 0, t)$ for $x \in [-L/2, L/2]$ and $t = 0, ..., T_{max}$.

All simulations have been performed by means of COMSOL Multiphysics® [26], a commercial code solving Partial Differential Equations based on the Finite Element Method (FEM). Apart from the different defect shapes, the model consists of an aluminum plate having a thickness of 40 mm, as in the experiment (see Section 4). The assumed physical properties of the plate are: thermal conductivity $\kappa = 237\ W/m^2K$, specific heat capacity $c = 900\ J/kgK$, density $\rho = 2700\ kg/m^3$. A value of the heat exchange coefficient h of $20W/m^2K$ is chosen to be compatible with the air flow produced by the commercial fan (actually a fume extractor) used in the laboratory experiments, amounting to $115m^3/min$. The external heat flux ϕ is assumed to be $1000W/m^2$.

Figure 1 shows the the value of the reconstructed $\epsilon\theta(x)$, computed by means of the inversion formula (16) as a function of time, for different defect widths and $\epsilon = 5mm$. The reconstruction is time-independent in both cases and we consider this fact a confirm of reliability of the method. While the third-order formula perfectly reconstructs a broad damage ($\gamma = 10^2 m^{-2}$), it appears to slightly underestimate the defect depth for a narrower one ($\gamma = 10^3 m^{-2}$). In both cases the dashed curve represents the actual defect (not visible in figure 1 (a)). It appears that the temperature contrast due to a smaller damage faster deteriorates with time, needing to retain a greater number of terms in the expansion (16).

The choice of a gaussian shape is less restrictive than it could seem. Indeed, damage shapes rather different from a gaussian bring to a gaussian-like reconstructions. This is as a consequence of the dissipative character of heat conduction. Something better can be done only if *a priori* information about the shape of the damage are available. Figure 2 shows the computed $\epsilon\theta(x)$ for $\theta = rect(x, d)$ with $d = 4cm$ (a) and $d = 20cm$ (b).

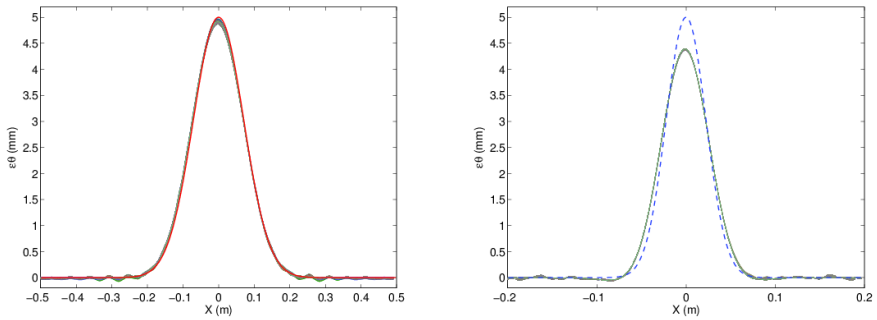

(a) (b)

Figure 1: Reconstructed $\epsilon\theta(x)$ for a gaussian defect having $\gamma = 10^2 m^{-2}$ (a) and $\gamma = 10^3 m^{-2}$ (b), as a function of the observation time

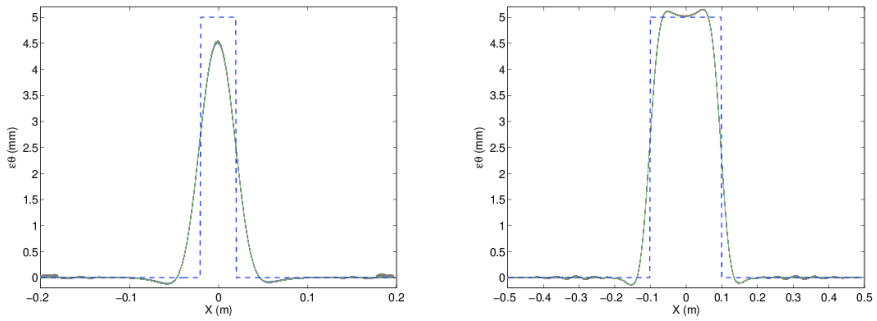

(a) (b)

Figure 2: Reconstructed $\epsilon\theta(x)$ for a rectangular defect having $d = 4cm$ (a) and $d = 20cm$ (b), as a function of the observation time

The inversion method also works well on damages of more complex shape. For example, figure 3 shows the reconstruction of a defect represented by the overlapping of two gaussian functions: $\epsilon\theta(x) = 5 \cdot 10^{-3} exp[-1500(x + 0.1)^2] + 2 \cdot 10^{-3} exp[-500(x - 0.1)^2]$. As before, the broader damage is quite perfectly reconstructed, although smaller in depth, while the narrower one is underestimated. However, the defect widths are correctly obtained and the inversion formula confirms to be independent on time.

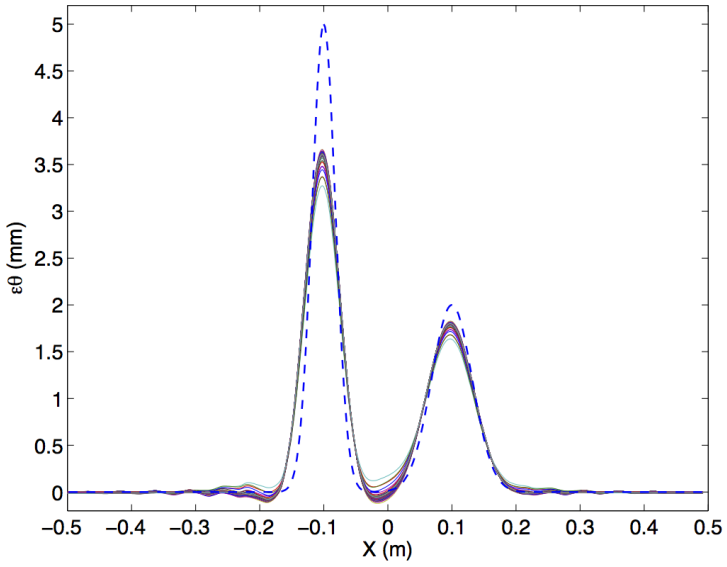

Figure 3: Reconstructed $\epsilon\theta(x)$ for a bimodal gaussian damage. The dashed curve represents the actual defect.

3 Determination of the heat flux density ϕ from thermal data

In section 1.1 we already pointed out that the flux density ϕ, though controlled in some sense, is actually unknown. Without a reliable estimate of ϕ we cannot apply our inversion method to real thermal data.

It comes from formula (4) that a constant flux ϕ_0 is determined by one temperature measurement taken in the first seconds. Assume now that ϕ is a generic smooth positive function so that it can be approximated by the trigonometric polynomial

$$\phi(x) = \phi_0 + \sum_{k=1}^{N} \left(\phi_{2k-1} cos \frac{2k\pi x}{L} + \phi_{2k} sin \frac{2k\pi x}{L} \right). \tag{17}$$

The coefficients ϕ_j for $j = 0, 1, ..., 2N$ can be recovered from the knowledge of the temperature $u(x, 0, t)$ measured on the accessible surface $z = 0$. In fact, let $u_j(z, t)$ be the solution of the one-dimensional IBVP

$$u_t = \alpha u_{zz} \tag{18}$$

$$\kappa u_z(a, t) + h(u(a, t) - U^0) = 0 \tag{19}$$

$$-\kappa u_z(0,t) = \phi_j \tag{20}$$

$$u(z,0) = U^0. \tag{21}$$

There is numerical evidence that for times t such that the "Fourier number" $t\alpha/a^2$ is small

$$u(x,0,t) \approx u_0(t) + \sum_{k=1}^{N} \left(u_{2k-1}(t) cos \frac{2k\pi x}{L} + u_{2k}(t) sin \frac{2k\pi x}{L} \right) \tag{22}$$

with:

$$\begin{aligned} u_0 &= \frac{\phi_0}{h} (1 + \lambda - \Sigma_N) + U_0 \\ u_j &= \frac{\phi_j}{h} (1 + \lambda - \Sigma_N) \end{aligned} \tag{23}$$

for $j = 0, 1, ..., 2N$, where λ, the β_k's and

$$\Sigma_N(t) = \sum_{k=1}^{N} \frac{2\lambda(\beta_k^2 + \lambda^2)}{\beta_k^2(\lambda + \lambda^2 + \beta_k^2)} e^{-\beta_k^2 \alpha t/a^2} \tag{24}$$

(a finite truncation of the series appearing in the analytical solution of the unidimensional problem (4)) are defined in 1.3.

Since we know $u(x,0,t)$ from our thermal measurements, we can compute the u_j's by means of the scalar products

$$\begin{aligned} u_0(t) &= \frac{1}{L} \int_{-L/2}^{L/2} u(x,t) dx \\ u_{2k-1}(t) &= \frac{1}{L} \int_{-L/2}^{L/2} u(x,t) cos \frac{2k\pi x}{L} dx \\ u_{2k}(t) &= \frac{1}{L} \int_{-L/2}^{L/2} u(x,t) sin \frac{2k\pi x}{L} dx. \end{aligned}$$

Finally, we invert relations (23) and determine the ϕ_j's. In particular, we get

$$\begin{aligned} \phi_0 &= \frac{(u_0(t) - U_0)h}{1 + \lambda + \Sigma_N(t)} \\ \phi_j &= \frac{u_j(t)h}{1 + \lambda + \Sigma_N(t)}. \end{aligned} \tag{25}$$

$$\tag{26}$$

We observe that the "theoretical" ϕ_j's are time-independent although they are infinite sums of the time-dependent quantities $u_j(t)$ and $lim_{N\to\infty}\Sigma_N(t)$.

We expect that the numerical approximations produced here are slightly dependent on t as a consequence of both the truncation of the series and the noise/uncertainty on the temperature data.

An independent, alternative way for computing the heat flux would therefore be appreciated as a validation tool.

A simple estimate of ϕ can be obtained by measuring the temperature behavior on a thermal insulating plate subjected to the same heat flux density ϕ. At short times, the low thermal conductivity allows to consider the problem as unidimensional, because the lateral diffusion is negligible and the heating of the plate is nearly adiabatic. The thermal energy $E(t)$ in the specimen, per unit width of the plate, is straightforwardly related to the integral of the temperature at time t over the plate thickness:

$$E(t) = \rho c \int_0^a (u(z,t) - U_0) dz \tag{27}$$

and the heat flux is computed from the energies at two close times t_1 and t_2:

$$\phi = \frac{\Delta E}{\Delta t} = \frac{E(t_2) - E(t_1)}{t_2 - t_1} \tag{28}$$

Of course, we cannot measure the temperature profile $u(z,t)$ inside the plate. The temperature measured on the accessible surface $z = 0$, $u(0,t)$ can be used to determine a depth δ at which $E(t) = \rho c(u(0,t) - U_0)\delta$. Such a depth can easily demonstrated to be related to the so-called *thermal penetration depth*:

$$\delta = \frac{1}{2}\sqrt{\pi \alpha t} \tag{29}$$

The above derivation is rigorously true when ϕ is constant, independent on x. At times t_1 and t_2 such that $\delta \ll a$, the heat flux is given by:

$$\phi = \frac{\sqrt{\pi}}{2} \left[\frac{(u(0,t_2) - U_0)\sqrt{t_2} - (u(0,t_1) - U_0)\sqrt{t_1}}{t_2 - t_1} \right] \sqrt{\kappa \rho c} \tag{30}$$

the last square root term being the effusivity of the insulating plate. The formula (30) can also be used in the case of a variable flux, $\phi = \phi(x)$, at times short enough to neglect the heat diffusion. Figure 4 compares the ϕ obtained from the series (17) with $N = 10$ with the approximation (30) for a true heat flux $\phi(x) = 470 - 1.2 \times 10^4 (x - L/2)^2$. Temperature data have been obtained on a simulated wooden plate of width $L = 1\,m$ and thickness $a = 8\,mm$, having thermal parameters $\kappa = 0.12\,Wm^{-1}K^{-1}$, $\rho = 500\,kg/m^3$, $c = 1760\,Jkg^{-1}K^{-1}$, and assuming $h = 5\,Wm^{-2}K^{-1}$ on the top surface of the plate.

In section 4 we will see how the above procedure is applied on real thermographic data.

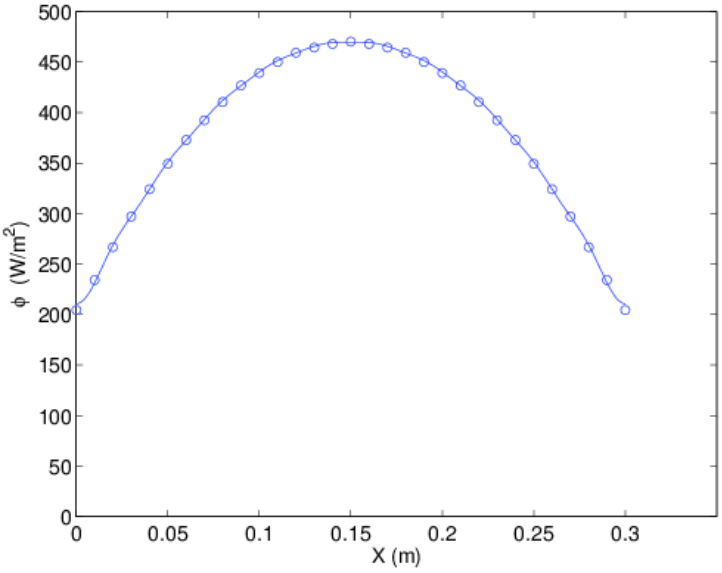

Figure 4: Comparison between ϕ reconstructed by the Fourier analysis (solid line) and the short-time approximation (circles)

4 Recovering the damage from real temperature measurements

The inversion method described in the previous sections has been tested on an aluminum plate having a thickness of 10 mm. This aluminum plate is a "thick" metallic object in the sense that it is very hard and far from being a foil. In the meanwhile, from the point of view of mathematical modeling, it is a "thin plate" because its thickness ($a = 10$ mm) is much lower than the size of external surfaces ($a \ll L \approx 200$ mm).

Two problems arise when trying to heat a bare metallic surface:

1. The very low emissivity (usually lower than 0.1 for a polished aluminum surface) prevents the material to be significantly heated.
2. The high reflectivity makes impossible to take thermographic images of the heated surface, because any object (including the heating lamps) is reflected into the thermographic camera.

The above well-known problems [23] are usually solved by covering the surface with a high-emissivity paint. Such an approach, while suitable in the laboratory, appears to be rather unpractical and usually too much invasive for a

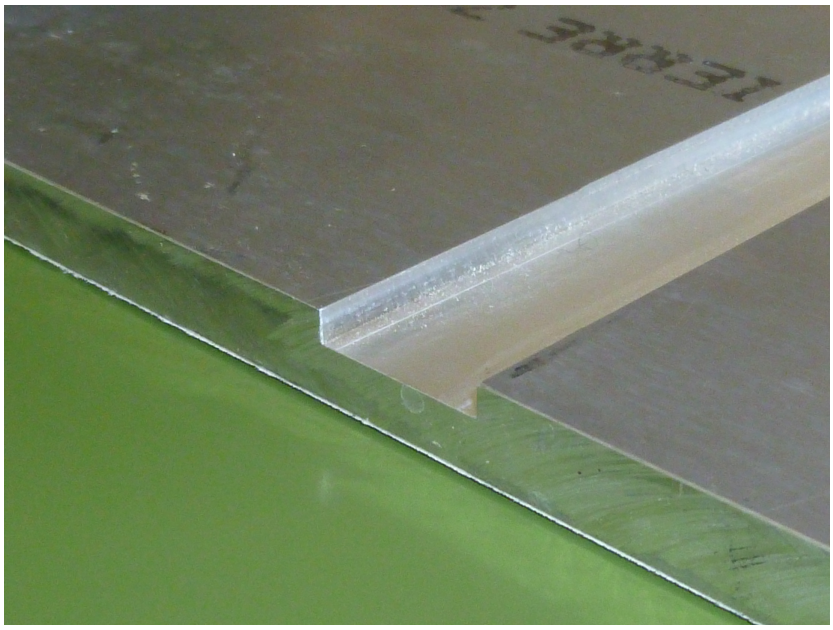

Figure 5: The damaged aluminum plate used for the experiment

real wall. Looking at published emissivity tables of common materials (e.g. [23], Table 8.1) matt paper appears to have an emissivity greater than 0.9. That suggested us the possibility of using an adhesive paper sheet to overcome the emissivity/reflectivity problem. That approach also modifies the thermal properties of the aluminum plate: the well known analogy among electrical and thermal circuits allows to treat the layered material paper/aluminum as an homogeneous medium having an effective thermal conductivity κ_e computed as the series of the individual conductivities:

$$\kappa_e = \frac{a + d_p}{\frac{d_p}{\kappa_p} + \frac{a}{\kappa}} \tag{31}$$

where d_p is the paper thickness, a is the thickness of the aluminum plate, κ_p and κ are the thermal conductivities of paper and aluminum, respectively. For a paper thickness of $8.2 \times 10^{-5} m$, assuming conductivities $\kappa_p = 0.08\, W m^{-1} K^{-1}$ and $\kappa = 237\, W m^{-1} K^{-1}$, the effective conductivity is about $9.5\, W m^{-1} K^{-1}$. The heat capacity and the density are computed according to the same electrical analog model, resulting very close to those of aluminum.

The damage consists in a rectangular slit of width 20 mm and depth 4 mm, as shown in figure 5.

Figure 6 shows the measurement setup. Two high-power spotlights ($1kW$ each) are placed and focalized such to produce a high heat flux density on the

Figure 6: The measurement setup

central region of the plate. The flux, as we will see in the following, has a parabolic shape. A thermographic image is acquired before the heating and for about 400 seconds after power on, at intervals of 5-6 seconds by means of a FLIR B335 thermal camera.

The thermographic images are successively processed by means of ThermaCAM Researcher® software, allowing to acquire the values on a given geometrical region, in particular over a horizontal line parallel to the wide side of the paper sheet, normal to the defect slit.

4.1 Heat flux estimate

The heat flux ϕ is estimated by taking a short series of thermographic shots on a plywood panel covered with a white matt painting, according to the procedure described in section 3.

Figure 7 compares the heat flux obtained by means of the Fourier analysis (solid lines) at times between 25 and 80 seconds with that computed using the short-time approximation based on the thermal penetration depth. The agreement between the two methods is very satisfactory, and the heat flux appears to be nearly parabolic in shape. Moreover, the flux is time-independent, as it should.

The heat flux could also be estimated by the temperature behavior measured on the target aluminum plate, at times small enough to ensure that the influence of the defect on the temperature distribution is negligible. Figure 8 shows that the reconstruction of ϕ is slightly time-dependent, but it is consistent with that obtained on the insulating panel. The computation based on measurements on a metallic plate is rather sensitive to the *true* value of the thermal conductivity of the material and on the heat exchange coefficient on the top surface.

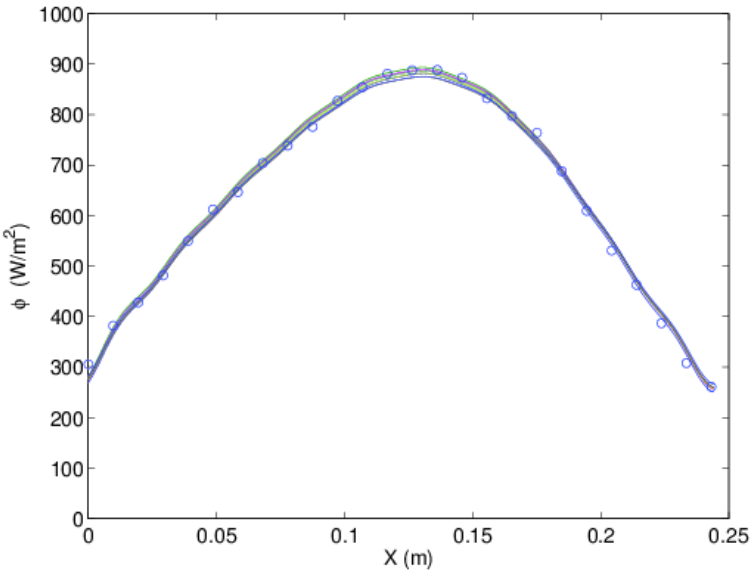

Figure 7: Heat flux measured on a plywood panel

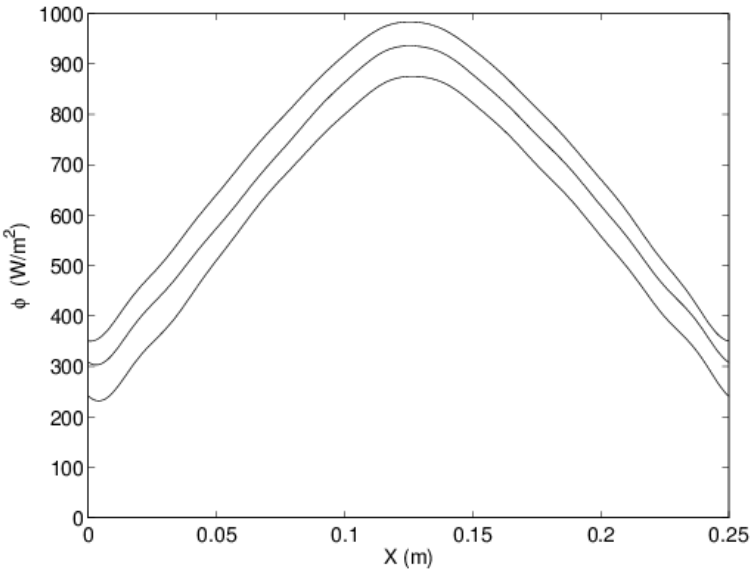

Figure 8: Heat flux measured on the aluminum plate with the defect

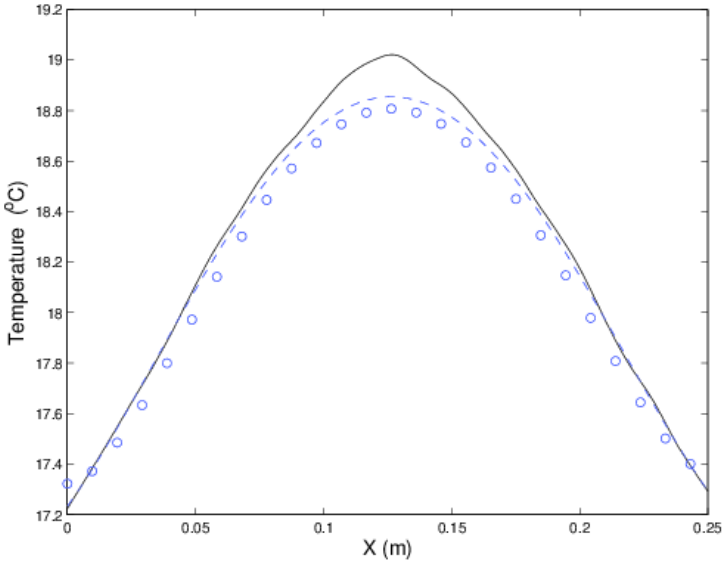

Figure 9: Temperature after 1 minute heating (solid line), compared to the fitted background (dashed line)

4.2 Defect detection

Figure 9 shows the temperature measured on a line crossing the defect, after 60 seconds heating (solid line). The background temperature (dashed line) is computed by fitting a polynomial to the lateral sides of the temperature distribution, i.e. excluding the central portion that is supposedly influenced by the defect on the opposite side. The background temperature could also be computed by simulating the experimental plate with the measured ϕ forcing term. That procedure gives reasonable results (circle symbols in figure 9) but as the computed temperature depends on the assumed physical parameters (thermal characteristics of the plate, heat exchange coefficient at the top surface), the "fitted" background appears to be more reliable and, incidentally, simpler to compute.

The thermal contrast, $u_\epsilon - u_0$ is then computed by subtracting the fitted background by the measured temperatures at every time. Figure 10 shows the contrast computed at time 60 seconds, from the data of figure 9. The position of the defect is clearly visible as a peak in the measured contrast.

The defect shape is recovered by applying the inversion formulas (15, 16). Figure 11 shows that the reconstructed $\epsilon\theta$ (solid lines) slightly depends on time, but nevertheless the correct position and order of magnitude for the true defect (dashed line) is obtained. The shape of the reconstructed defect is gaussian-like

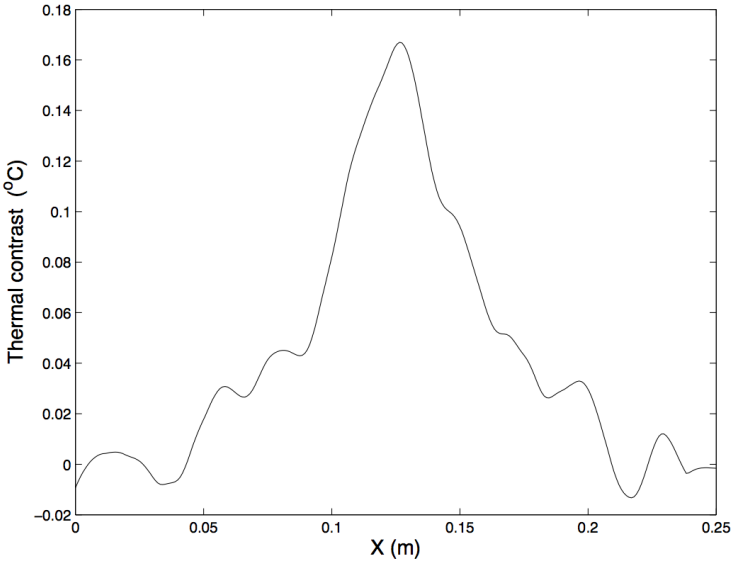

Figure 10: Contrast after 1 minute heating

as observed with simulated data.

The experimental situation shown in figures 9 to 11 is somehow *ideal*, because the heating maximum is centered on the known position of the defect. A procedure for detecting a defect on a metal plate would be based on scanning the surface by varying the position of the maximum heating. Figure 12 shows the temperature measured after 60 seconds heating, when the heating lamps are oriented such to have a maximum at the right of the defect axis. The temperature distribution has a slightly asymmetric shape (perfectly reproduced in numeric simulations), giving rise to a thermal contrast like that shown in figure 13, where the horizontal axis has been limited to a smaller range around the maximum to emphasize the appearance of an asymmetrical smaller peak at the right of the defect, due to the heating maximum.

The reconstruction of the defect is however possible also with an off-center illumination, as figure 14 shows. The appearance of a spurious *tail* on the right of the true defect is due to the *wrong* illumination, but the size of the defect is properly obtained.

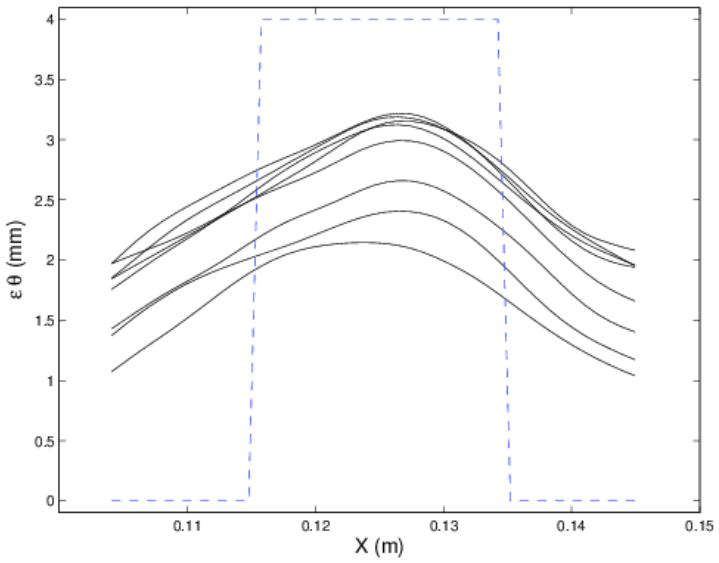

Figure 11: Defect (solid lines) reconstructed at times between 30 and 75 seconds, compared to the true defect (dashed line)

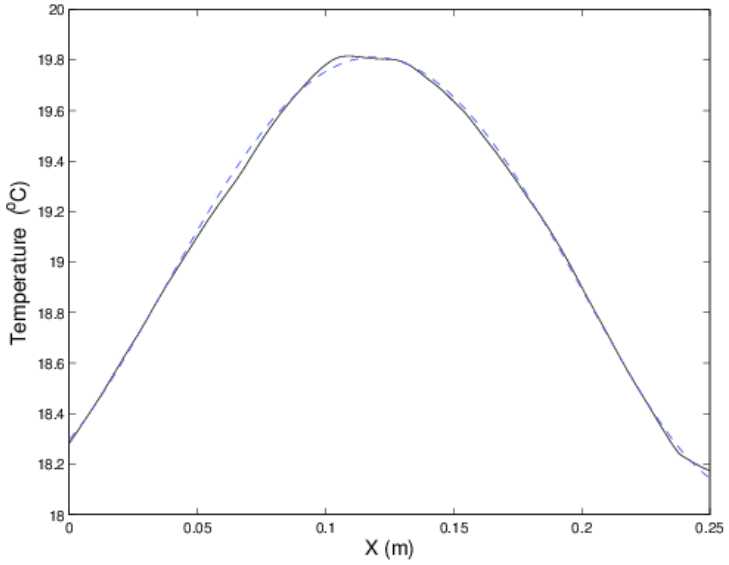

Figure 12: Temperature after 1 minute off-center heating (solid line), compared to the fitted background (dashed line)

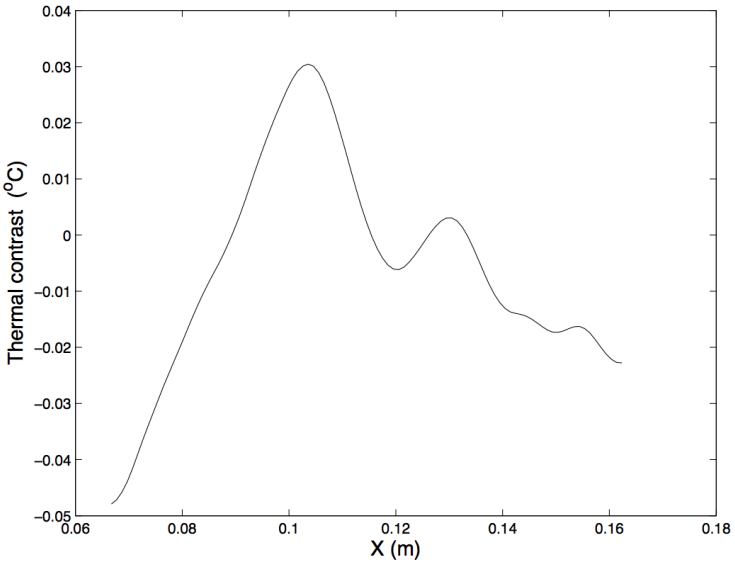

Figure 13: Contrast after 1 minute off-center heating

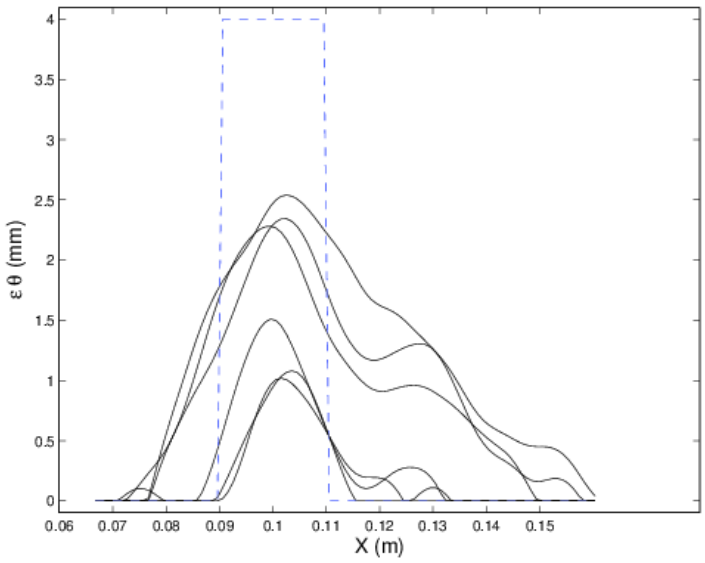

Figure 14: Defect (solid lines) reconstructed at times between 30 and 75 seconds for off-center heating, compared to the true defect (dashed line)

Appendix. Thin Plate Approximation and Perturbation Theory. The special case of two-dimensional domain and flux Φ constant in x e t

If the function θ is "cylindrical" (i.e. $\theta(x,y) = \theta(x)\ \forall y \in [-\frac{L}{2}, \frac{L}{2}]$), for large values of L, problem **IP'** is essentially a two dimensional one. It happens, in particular, when the defected region unevenly develops along one of the coordinates, as shown in figure 15. In this section, we use 2D Thin Plate Approximation (TPA) (see [22], [18], [19]) to build an approximate explicit formula for the reconstruction of the damage $\epsilon\theta$.

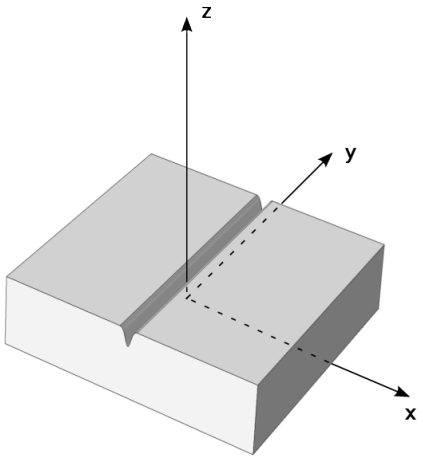

Figure 15: A "cylindrical" geometry justifying the 2D approach

If we have no *a priori* information about the localization of the damage it is natural to use a heat flux constant in both space and time variables. Hence, the background temperature u^0 is independent of x and will be written as $u^0(z,t)$. In this case, inversion formulas turns out to be much simpler that the general 2D and 3D cases reported in Appendix. Although, it is not easy to produce a spatially constant heat flux, we will see in the numerical section 2 that "equivalent" constant fluxes give very accurate reconstructions.

First of all, we change the variable z so that the thickness of the domain remains equal to one when a goes to zero in the Thin Plate Approximation: we rescale z and transform it in the new variable $\zeta = \frac{z}{a}$.

Since $w_\zeta = \frac{w_z}{a}$ we get the following IBVP for domain derivative

$$\frac{a^2}{\alpha} w_t = a^2 w_{xx} + w_{\zeta\zeta}$$

$$\kappa w_\zeta(x,1,t) + ahw(x,1,t) = a\epsilon\theta(x)(hu_z^0(a,t) + c\rho u_t^0(a,t))$$

$$\kappa w_\zeta(x,0,t) = 0$$

$$w_x(-L/2,\zeta,t) = w_x(L/2,\zeta,t) = 0$$

(i.e. adiabatic conditions on the vertical sides) and $w(x,\zeta,0) = 0$ (initial condition).

Moreover, we have the extra boundary condition

$$w(x,0,t) \approx u^\epsilon(x,0,t) - u^0(0,t)$$

obtained in practice by means of an infrared camera and necessary for the reconstruction of $\epsilon\theta$. The notation

$$D(t) = hu_z^0(a,t) + c\rho u_t^0(a,t)$$

will be useful in what follows.

We expand formally w and θ

$$w = w_0 + aw_1 + a^2 w_2 + O(a^3)$$

$$\theta = \theta_0 + a\theta_1 + a^2\theta_2 + O(a^3),$$

and plug the expansions into the IBVP.

Order zero We have

$$w_{0\zeta\zeta} = 0$$

with $w_{0\zeta}(x,1,t) = w_{0\zeta}(x,0,t) = 0$ so that $w_0(x,\zeta,t) = w_0(x,0,t)$ for all $\zeta \in [0,1]$.

Order one We have

$$w_{1\zeta\zeta} = 0$$

with

$$\kappa w_{1\zeta}(x,1,t) + hw^0(x,1,t) = \epsilon\theta_0(x)D(t)$$

and

$$w_{1\zeta}(x,0,t) = 0.$$

Since $w_{1\zeta}(1) = w_{1\zeta}(0) + \int_0^1 w_{1\zeta\zeta}(\zeta)d\zeta = 0$, we have that also w_1 is independent of ζ and

$$\epsilon\theta_0(x,t) = \frac{hw^0(x,t)}{D(t)}. \tag{32}$$

Order two

We have

$$w_{2\zeta\zeta} = \frac{w_{0t}}{\alpha} - w_{0xx}.$$

Since w^0 is independent on ζ, we have

$$w_2(x,\zeta,t) = (\frac{w_{0t}(x,t)}{\alpha} - w_{0xx}(x,t))\frac{\zeta^2}{2}. \tag{33}$$

Observe that, from (33) we have $w_2(x,0,t) = 0$ for all x and t. For $n \geq 2$ we have

$$w_{n+1_{\zeta\zeta}} = \frac{w_{n-1_t}}{\alpha} - w_{n-1_{xx}} = G_{n-1}(x,t)\frac{\zeta^{n-1}}{(n-1)!} \tag{34}$$

so that, for $n \geq 2$

$$w_n(x,0,t) \equiv 0. \tag{35}$$

Hence,

$$w_0(x,0,t) + aw_1(x,0,t) = w(x,0,t) \approx u^\epsilon(x,0,t) - u^0(x,0,t).$$

A setting of w^0 and w^1 compatible with (35) is $w_0(x,0,t) = w(x,0,t)$ and $w_1(x,0,t) \equiv 0$. It means that $w_1(x,\zeta,t) \equiv 0$ in $\Omega_0 \times (0,T_{max}]$. Also $w_3 \equiv 0$ (from (34). It is easy to prove by induction that $w_{2n+1} \equiv 0\ \forall n = 1,2,3,....$

Hence, on the top boundary of the rectangle, we have

$$\kappa w_{2\zeta} = \epsilon\theta_1 D(t) = \kappa\int_0^1 (\frac{w_{0t}}{\alpha} - w_{0xx})dx$$

and, consequently,

$$\epsilon\theta_1(x,t) = \frac{c\rho w_{0t}(x,t) - \kappa w_{0xx}(x,t)}{D(t)}. \tag{36}$$

Order three

We have

$$\kappa w_{3\zeta}(x,1,t) + hw_2(x,1,t) = \epsilon\theta_2(x)D(t) \tag{37}$$

Since w_3 vanishes everywhere we have

$$\epsilon\theta_2(x,t) = \frac{h}{2\kappa}\frac{c\rho w_{0t} - \kappa w_{0xx}}{D}. \tag{38}$$

Order four

Since

$$\kappa w_{4\zeta}(x,1,t) + h w_3(x,1,t) = \epsilon\theta_3(x)D(t) \tag{39}$$

we have

$$\epsilon\theta_3(x,t)D(t) = \kappa \int_0^1 (\frac{w_{2t}(x,t)}{\alpha} - w_{2xx}(x,t))dz. \tag{40}$$

Since

$$\frac{w_{0t}(x,t)}{\alpha} - w_{0xx}(x,t)) = \frac{D(t)\epsilon\theta_1(x)}{\kappa} \tag{41}$$

we have $w_2(x,\zeta,t) = \frac{D(t)\epsilon\theta_1(x,t)}{\kappa}\frac{\zeta^2}{2}$ so that

$$\epsilon\theta_3(x,t) = \frac{1}{6\alpha}(\epsilon\theta_{1t}(x,t)D(t) + \epsilon\theta_1(x,t)D_t(t)) - \frac{1}{6}D\epsilon\theta_{1xx}(x,t). \tag{42}$$

Remark about non constant flux Although in practice we can use a constant "equivalent" flux density (see section 4), equations for $\theta_k(x,t)$ can be written also for $\phi = \phi(x)$. In this case, instead of algebraic relations like (32) or (36) we have ordinary differential equations of the first order, due to the presence of the derivative θ_x in the boundary conditions of domain derivative (see (6).

If we are modeling the full dimensional problem in which $\phi = \phi(x,y)$, the damage $\epsilon\theta$ solves a linear partial differential equation of the first order. These differential equations can be solved analytically, but they require a special care in the neighborhood of possible maxima of the temperature where the equation cannot be written in normal form. Although this is still a work in progress, in figure 16 we show the reconstruction of a synthetic damage (green line) detected in 2D with a non constant flux solving a ODE in singular implicit form (continuous blue line) compared with the solution obtained with constant equivalent flux density (dashed line).

5 Conclusions

In this paper we derive formally an explicit approximation of the solution of a nonlinear inverse problem for the heat equation on a thin conducting plate. More precisely, we recover an inaccessible surface damage $\epsilon\theta$ from thermal data. First we linearize the direct model by means of Domain Derivative. Then, we use perturbation theory in order to construct the Thin Plate Approximation of $\epsilon\theta$ at the first order. Finally, we test the reconstruction strategy with real thermal data.

References

[1] H. I. Syed, W. Winfree, E. Cramer, P. A. Howell Thermographic Detection of Corrosion in Aircraft Skin in "Review of Progress in Quantitative Nondestructive Evaluation" DOI: 10.1007/978-1-4615-2848-7, 2035-2041 (1993)

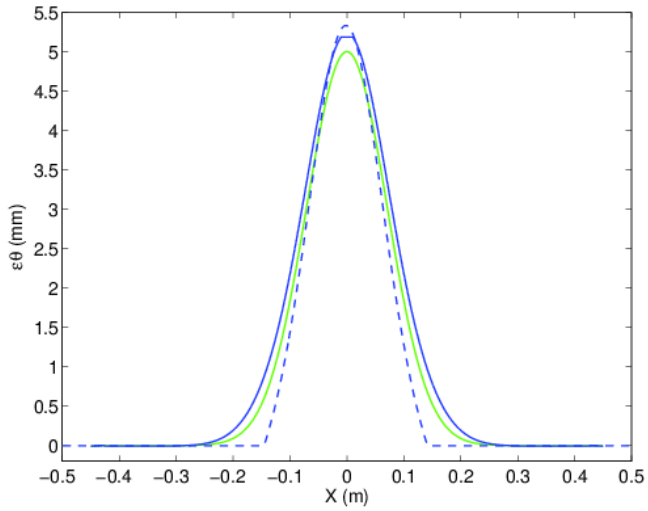

Figure 16: Damage reconstruction in the variable flux case

[2] K. E. Cramer, P. A. Howell, H. I. Syed Quantitative thermal imaging of aircraft structures Proc. SPIE Thermosense XVII, 2473, 226232 (1995)

[3] J. Hyun Kim, K. Hwan Yoo, M. Gyun Na, J. Weon Kim, K. Suk Kim On-power detection of pipe wall-thinned defects using IR thermography in NPPS Nuclear Engineering and Technology Volume 46, Issue 2, 225234 (2014)

[4] T. Sakagami, Y. Izumi, Y. Kobayashi, Y. Mizokami, S. Kawabata Applications of infrared thermography for nondestructive testing of fatigue cracks in steel bridges Proc. SPIE 9105, Thermosense: Thermal Infrared Applications XXXVI, 91050S, doi: 10.1117/12.2057382 (2014)

[5] E. Grinzato, V. Vavilov, P. Bison, S. Marinetti Hidden corrosion detection in thick metallic components by transient IR thermography Infrared Phys. Technol. (49) (2007), pp. 234238

[6] V. Vavilov, A. Chulkov Detecting corrosion in thick metals by applying active IR thermography Proc. of SPIE, Vol. 8354, 2012, DOI: 10.1117/12.920321

[7] J V Back, B Blackwell and C A St.Clair, *Inverse Heat Conduction - Ill posed Problems* Wiley, New York (1985).

[8] H. T. Banks, F. Kojima and W. P. Winfree, Boundary estimation problems arising in thermal tomography. *Inverse Problems* **6**, 897–921 (1990).

[9] P.Bison, M.Ceseri, D.Fasino and G.Inglese *Domain derivative approach to Active InfraRed Thermography*, Inverse Problems in Science and Engineering 18:7, 873-889 (2010).

[10] K. Brian and L. F. Caudill, Reconstruction of an unknown boundary portion from Cauchy data in n dimensions. *Inverse Problems* **21**, 239–255 (2005).

[11] V. Bacchelli, S. Vessella, Lipschitz stability for a stationary 2D inverse problem with unknown polygonal boundary, Inverse Problems 22, (2006), 1627-1658.

[12] Bacchelli V, Veneziani A and Vessella S 2010 Corrosion detection in a 2D domain with a polygonal boundary *J.Inv.Ill-Posed Problems* 18 281-305

[13] H. S. Carslaw and J. C. Jaeger, *Conduction of Heat in Solids.* Oxford University Press (1959).

[14] W.S. Cleveland, Robust Locally Weighted Regression and Smoothing Scatter- plots, J. Amer. Statist. Assoc. 74 (1979), 829836.

[15] H. W. Engl, M. Hanke and A. Neubauer, *Regularization of Inverse Problems*. Kluwer Accademic Publisher (2000).

[16] D Fasino, G Inglese and F Mariani, Corrosion detection in conducting boundaries: II. Linearization, stability and discretization Inverse Problems 23 (2007) 1101-1114.

[17] F Hettlich and W Rundell, Identification of a discontinuous source in the heatequation Inverse Problems, Volume 17, Number 5 (2001), 1465-1482.

[18] G.Inglese, *An inverse problem in corrosion detection* Inverse Problems **13** (1997), 977–994.

[19] G Inglese and R Olmi, *Nondestructive evaluation of inaccessible surface damages by means of active thermography* Rend. Istit. Mat. Univ. Trieste Volume 48 (2016)

[20] V. Isakov, On uniqueness of obstacles and boundary conditions from the dynamical data, Inverse Probl. Imaging 2 (2008) 151-65

[21] D.A. Jones, *Principles and Prevention of Corrosion* Englewood Cliffs, NJ: Prentice -Hall (1996).

[22] P.G. Kaup, F. Santosa, M. Vogelius. Method for imaging corrosion damage in thin plates from electrostatic data. Inverse Problems, 12 (1996), pp. 279293.

[23] X. P. V. Maldague, *Theory and Practice of Infrared Technology for Nondestructive Testing*. J. Wiley and Sons, (2001), New York.

[24] S. Salsa, *Partial Differential Equations in Action* Springer, Milano, 2008.

[25] Simon J, *Differentiation with respect to the domain in boundary value problems*, Numer. Funct. Anal. Optim., 2(1980), 649-687.

[26] COMSOL Multiphysics® v. 5.2. www.comsol.com. COMSOL AB, Stockholm, Sweden.